Difficulties in Defining the Degree of Superheat in Flash Boiling Liquid Nitrogen Sprays

Andreas Rees*[1], Michael Oschwald[1,2], Jan Wilhelm Gärtner[3], Andreas Kronenburg[3]

[1]German Aerospace Center (DLR), Institute of Space Propulsion, Langer Grund, Hardthausen 74239, Germany

[2]RWTH Aachen University, Institute of Jet Propulsion and Turbomachinery, Templergraben 55, Aachen 52062, Germany

[3]University of Stuttgart, Institute for Combustion Technology, Herdweg 51, Stuttgart 70174,

*Corresponding author email: Andreas.Rees@dlr.de

Abstract

Technology development for propulsion systems of upper stages and reaction control thrusters is driven by green propellants to substitute hydrazine. At high-altitude conditions prior to ignition the liquid propellants are injected into the combustor at near-vacuum. Due to the sudden pressure drop the liquid is in a superheated thermodynamic state resulting in an eruptive evaporation and fast expansion, a process called flash boiling. To know the composition related to phase and atomization is important for both to determine the probability of a successful ignition and to avoid destructive pressure peaks. Hence, we visualized flash boiling liquid nitrogen (LN2) sprays by means of shadowgraphy at the cryogenic test bench M3.3 at DLR. The data analysis of these sprays revealed that the commonly used degree of superheat Rp on its own is not sufficient to describe the flash boiling process. This paper focuses on the description of this issue by comparing shadowgraph images of different LN2 sprays to each other and by the discussion of the kinetics of the sprays in terms of velocity and pressure distributions obtained by numerical simulation. Despite similar degrees of superheat Rp, the spray morphology as well as the spray kinetics show serious deviations from each other.

Keywords

Flash boiling, degree of superheat, cryogenic, atomization.

Introduction

Technology development for propulsion systems of upper stages like the cryogenic Ariane 6 upper stage engine Vinci or for future cryogenic thrusters in reaction control or orbital and manoeuvring systems is driven by the invention of new, green propellants to substitute hydrazine, and by new ignition technologies like laser ignition [1]. At high-altitude conditions prior to ignition the liquid propellants are injected into the combustor at near-vacuum conditions. This means that the ambient pressure p_a is lower than the liquid's saturation pressure $p_{sat}(T_{inj})$ at the injection temperature T_{inj}. The sudden pressure drop at injection leads to a superheated liquid in a metastable thermodynamic state. The injection of a liquid like that results in a fast expansion and eruptive evaporation, a process called flash boiling or flash evaporation. The evaporating gases raise the pressure inside the combustion chamber until the equilibrium pressure shortly before ignition is reached. To know the composition of the propellants in the combustion chamber related to phase, species and temperature distribution is important for determining the parameters for a successful ignition and for avoiding destructive pressure peaks.

Flash Boiling

The dominating parameters for the flash boiling phenomenon in a given liquid are the injection temperature T_{inj} and the back pressure p_{ch} which can be a near-vacuum chamber pressure or atmospheric conditions. According to Figure 1, they both define the dimensionless degree of

superheat R_p of the injected liquid in terms of the pressure ratio

$$R_p = \frac{p_{sat}(T_{inj})}{p_{ch}}, \tag{1}$$

with the saturation pressure $p_{sat}(T_{inj})$ at the injection temperature T_{inj} and the back pressure p_{ch}. A superheated liquid jet with a high degree of superheat is atomized close to or already in the injector nozzle due to vaporization and produces a fine spray with a big opening angle and small droplets. The influence of aerodynamical processes on the primary atomization can be neglected in this kind of jets [2]. The vaporization and expansion of a flash boiling spray leads to a cool-down to reach a new equilibrium state at the saturation temperature $T_{sat}(p_{ch})$.

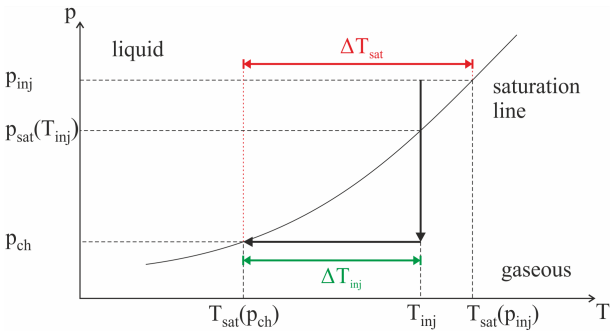

Figure 1. Phase diagram of a superheated liquid for adiabatic depressurization

State of Research

In the last three decades there have been increased efforts of the automotive industry to investigate flash boiling processes of storable liquids typical for the injection into gasoline or diesel engines [3, 4]. Pre-heating the fuel to reach the superheated condition causes flash boiling during the injection which leads to a finer and wider atomization in the combustion chamber. This increases the efficiency and reduces exhaust emissions [4]. Analytical models were developed for flash boiling hydrocarbon sprays to predict the nucleation rates and resulting droplet sizes [3] and for water sprays to predict the liquid superheat with the help of the depressurization transient [5]. Further studies about flash boiling processes can be found concerning the safety field in process technology or chemical and nuclear industry, where storable fluids like hydrocarbons, water, ethanol or refrigerants like R-134A were used [5, 6, 7]. It was found that not only the degree of superheat determines the intensity of flash boiling but also injection conditions like the injection pressure or the injector diameter [7]. Transition correlations depending on the dimensionless Weber and Jakob numbers were empirically developed for superheated water leaking into the atmosphere to subdivide the resulting sprays into an aerodynamical break-up region, a transition region and a fully flashing region [6]. The validity range of these correlations was successfully expanded for the fluids iso-octane, acetone and ethanol [8]. In the same study an onset criterion, which links flash boiling with the classical nucleation theory, for the flashing regimes was developed, and a model for predicting the spray angle in the near-nozzle region by the degree of superheat and the dimensionless surface tension was generated. In contrast to storable fluids, flash boiling of cryogenic liquids is much less investigated due to significantly harder experimental conditions. Within an experimental study at DLR Lampoldshausen about laser ignition in a model rocket combustion chamber at high-altitude conditions, flash boiling was observed for a liquid oxygen (LOX) jet [9]. At the same test bench flash boiling of LOX jets with two injection configurations was investigated and the results were compared to flash boiling sprays of storable fluids [10]. Despite the huge differences in their physical properties the LOX sprays and the sprays with storable liquids showed a similar spray morphology. In another experimental study about cryogenic flash boiling, sprays of liquid nitrogen (LN2) for injection times of about 10 s were observed with high-speed shadowgraphy for different injection conditions and injector geometries [11]. The resulting sprays showed maximum spray angles

of about 140° and the injector geometry and injection pressure did not have big influences on the spray angles. In the former work [12] the validity range of the transition correlations from [6] was successfully expanded for the cryogenic fluid LN2 and an asymptotical evolution of the spray angle with increasing superheat was shown. In a consecutive study, the droplet velocity and diameter distributions of highly superheated flash boiling LN2 sprays with constant injection conditions were measured by means of PDA and preliminary results like possible recirculation zones or the existence of a second droplet population were shown [13]. A subsequent in-depth data analysis of this measurement campaign showed, that the droplet velocity and diameter distributions of flash boiling LN2 sprays have a sufficient degree of similarity with data of storable fluids from literature [14]. In a former study [15], the characteristic morphology like break-up patterns and spray angles of flash boiling LN2 sprays was determined by means of high-speed shadowgraphy in dependence on the injection parameters and derived dimensionless quantities. Similar to storable fluids, increasing degrees of superheat lead to a growing dominance of flash boiling on the break-up of the liquid nitrogen jet. Hence, correlations about jet break-up regimes derived for storable fluids showed their suitability for cryogenic nitrogen as well. In reference [16] it was shown, that existing models to predict the dimensions of the liquid cores in flash boiling LN2 sprays are only applicable for low degrees of superheat.

Experimental Set-Up

Since the dominating parameters for flash boiling are the injection temperature T_{inj} and the back pressure p_{ch}, it is important for an experimental investigation to make them adjustable, to keep them constant during the injection period and to make them reproducible. This is why the new test bench M3.3 with a temperature-controlled injection system was built at DLR Lampoldshausen for a detailed experimental investigation of cryogenic flash boiling processes [12, 13, 14, 15, 16].

Cryogenic Test Bench M3.3

The test bench M3.3 consists of three main systems, as depicted in Figure 2: the media supply and pressurization system, the cryogenic temperature adjustment and injection system (CTAIS) and the vacuum system. With the first system all gases (nitrogen, helium) for the operation of the test bench are provided and are pressurized with various pressure reducers to the desired pressures. The second of the three main systems consists of a double-walled and vacuum-insulated pressure tank filled with liquid and gaseous nitrogen (GN2), see Figure 2 on the left and right. By an evacuation or pressurization of the GN2 phase in the pressure tank the fluid is cooled down or heated up, respectively. Inside the pressure tank is the complete LN2 feed and injection system, which consists of a 0.5 liter LN2 run-tank, a coriolis mass flowmeter, the injector unit with a pneumatic run valve and the injector nozzle, and piping in-between, see Figure 2 in the middle. That means that all these sub-systems are completely surrounded by the cooling medium nitrogen to provide a homogeneous temperature distribution from the run-tank to the injector nozzle. Several dynamic pressure and temperature sensors are installed at the nitrogen pressure tank as well as at the feed and injection system, in order to both control and adjust the temperature of the cooling medium and to measure the injection parameters of the jets. The CTAIS is mounted on top of the vacuum system, which consists of a cylindrical chamber with an inner diameter of 300 mm, a height of 225 mm from the injector nozzle exit to the bottom of the chamber and four optical accesses with a diameter of 100 mm each. The four windows are positioned with an angle of 90° to each other. An attached vacuum pump produces the near-vacuum atmosphere to simulate high-altitude conditions. The test fluid nitrogen gets liquefied during the chill-down process of the test bench. Further details about the test bench M3.3 and its possible range of injection conditions can be found in references [12, 13, 14, 15].

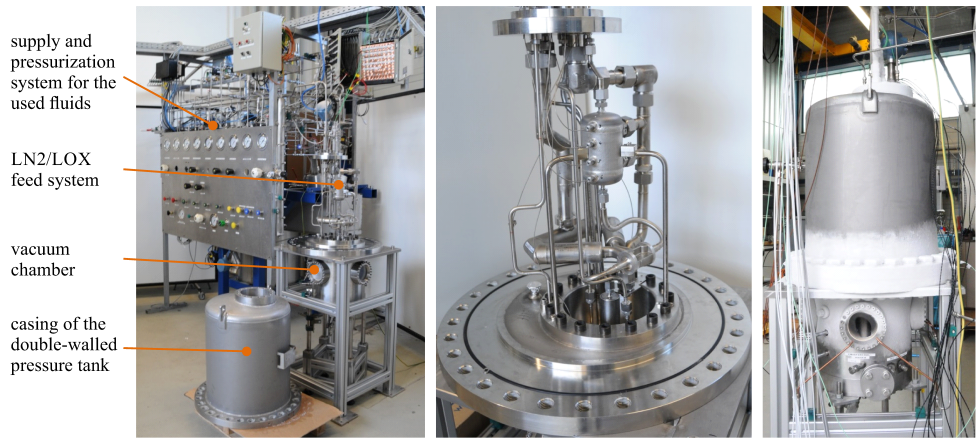

Figure 2. Test bench M3.3 with supply and pressurization system, open CTAIS and vacuum system (left); open CTAIS with run tank, pneumatic run valve, injector unit and sensors in-between (middle); chilled-down test bench in operation mode (right) [14]

Injection Conditions

In this study, we are using the four LN2 sprays #1, #6, #9 and #14 which were generated by a single sharp-edged injector with a diameter of $D_{inj} = 1$ mm and a length-to-diameter ratio of $L/D = 2.9$. For further injector details we refer to former works [12, 13, 14, 15, 16]. The injection conditions in terms of the injection temperature T_{inj}, the injection pressure p_{inj}, the chamber pressure p_{ch}, the mass flow $\dot{m}$, the degrees of superheat R_p and ΔT^* as well as the dimensionless numbers like the gaseous and liquid Weber numbers We_g and We_l, respectively, the Jacob number Ja, the Reynolds number Re and the Ohnesorge number Oh of the sprays #1, #6, #9 and #14 are summarized in Table 1. Detailed definitions of these numbers as well as their confidence intervals can be found in reference [15].

	#1	#6	#9	#14
T_{inj} [K]	82.9	82.9	82.6	82.7
p_{inj} [kPa]	820	800	400	410
p_{ch} [kPa]	61	26	60	26
$\dot{m}$ [g/s]	17.2	17.2	9.8	9.8
R_p [-]	3.0	7.0	3.0	7.0
ΔT^* [-]	0.350	0.466	0.520	0.636
We_g [-]	298.9	136.9	95	43.8
Ja [-]	27.9	69.9	27.7	97.2
We_l [-]	8.06×10^4	8.02×10^4	2.59×10^4	2.59×10^4
Re [-]	1.66×10^5	1.66×10^5	9.45×10^4	9.45×10^4
Oh [-]	1.71×10^{-3}	1.71×10^{-3}	1.70×10^{-3}	1.70×10^{-3}

Table 1. Injection conditions of the analysed LN2 sprays #1, #6, #9 and #14

Optical Diagnostics

High-speed backlight shadowgraphy was used to visualize the flash boiling LN2 sprays. With a xenon light source, the sprays were illuminated from the backside through one of the four optical accesses of the vacuum chamber. A translucent frosted glass was placed between the light source and the chamber window to provide a homogeneous background. The high-speed camera was positioned on the opposite optical access of the chamber and the camera lens was focussed onto the injector plane prior to each test run. The optical set-up is shown schematically in Figure 3. Its main components as well as the settings of the used high-speed camera are listed in Table 2. The evolution of the injection pressure showed that after a period of about $t_{inj} = 100$–120 ms after the trigger signal for the injection start steady state injection

conditions are reached [15]. Hence, we chose $t_{inj} = 120$ ms as evaluation time, where all of the shown shadow-graph images in this study were analysed.

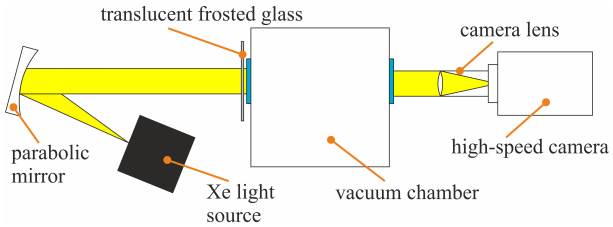

Figure 3. Scheme of the optical set-up for high-speed backlight shadowgraphy at test bench M3.3 [15]

component/parameter	manufacturer and type/setting
xenon light source	Müller Elektrik & Optik, SVX 1450 & LAX 1450
camera lense	Tamron, A061 AF28-300mm
camera	Photron Fastcam SA-X
framerate	10 000 fps
exposure time	97 µs
frame size	1024×1024 pixels

Table 2. Components of optical shadowgraphy set-up at test bench M3.3

Numerical Set-Up

To investigate the spray kinematics and the flow in the injector nozzle, 2D simulations of the four cases, with a grid size of 10 µm, are set up, see also Figure 5. The flashing nitrogen flow is solved with a compressible two-phase, one component solver developed in OpenFOAM [17]. The solver has already been applied to flashing flows and has proven its suitability to predict flashing sprays.

Governing Equations

The selected solver uses an Euler-Euler approach with a transport of a volume fraction to distinguish between the two phases. Thus, additional to the momentum, mass and energy conservation, a transport of the liquid volume fraction is included,

$$\frac{\partial \bar{\rho}_\mathrm{l}\widetilde{\alpha}}{\partial t} + \nabla \cdot (\bar{\rho}_\mathrm{l}\widetilde{\alpha}\widetilde{\boldsymbol{u}}) + \nabla \cdot (\overline{\rho_\mathrm{l}\alpha_\mathrm{l}''\boldsymbol{u}''}) = \widetilde{\dot{m}_\mathrm{l}}, \tag{2}$$

$$\frac{\partial \bar{\rho}\widetilde{\boldsymbol{u}}}{\partial t} + \nabla \cdot (\bar{\rho}\widetilde{\boldsymbol{u}}\widetilde{\boldsymbol{u}}) = -\nabla \bar{p} + \bar{\rho}g + \nabla \cdot \widetilde{\boldsymbol{\tau_t}}, \tag{3}$$

$$\bar{\rho}\frac{\mathrm{D}\widetilde{h}_\mathrm{l}}{\mathrm{D}t} + \bar{\rho}\frac{\mathrm{D}\widetilde{K}}{\mathrm{D}t} = \left(\frac{\partial \bar{p}}{\partial t} + \nabla \cdot (k_{\mathrm{l,Eff}}\nabla \widetilde{T}_\mathrm{l})\right) + \frac{\bar{\rho}}{\bar{\rho}_\mathrm{l}\bar{\alpha}_\mathrm{l}}\dot{m}_\mathrm{l}(h_{\mathrm{sat,g}}(p) - \widetilde{h}_\mathrm{l}), \tag{4}$$

$$\bar{\rho}\frac{\mathrm{D}\widetilde{h}_\mathrm{g}}{\mathrm{D}t} + \bar{\rho}\frac{\mathrm{D}\widetilde{K}}{\mathrm{D}t} = \left(\frac{\partial \bar{p}}{\partial t} + \nabla \cdot (k_{\mathrm{g,Eff}}\nabla \widetilde{T}_\mathrm{g})\right) + \frac{\bar{\rho}}{\bar{\rho}_\mathrm{g}\bar{\alpha}_\mathrm{g}}\dot{m}_\mathrm{l}(\widetilde{h}_\mathrm{g} - h_{\mathrm{sat,g}}(p)), \tag{5}$$

Hereby, the subscripts 'l' and 'g' denote the liquid and vapor phase, whereas variables without a subscript refer to the mixture properties. Variables with an overbar, $\bar{\phi}$, denote Reynolds averaged quantities, whereas the tilde denotes Fave averaging and the double prime their fluctuations. The turbulence is modeled with the k-ω SST model and the turbulent contributions for the enthalpy transport equations are included in the effective thermal conductivity using the turbulent Prandtl number. To get the superheated as well as the saturation properties the CoolProp library is used as the equation of state [18].

Phase Change Model

In comparison to cavitation, flashing cannot be assumed to be in thermal equilibrium and therefore the homogeneous relaxation model (HRM), which uses an empirical relaxation time

$$\Theta = \Theta_0 \left(\frac{\rho_\mathrm{l} - \rho}{\rho_\mathrm{l} - \rho_\mathrm{g}} \right)^{\beta} \left(\frac{p_{sat}(T) - p}{p_{sat}(T)} \right)^{\lambda}, \tag{6}$$

is used to describe the evaporation rate [19, 20]. The final expression for the phase change with χ as the liquid mass fraction is then,

$$\frac{\mathrm{D}\chi}{\mathrm{D}t} = -\chi \frac{h_\mathrm{l}(p,T) - h_{\mathrm{sat,l}}(p)}{h_{\mathrm{sat,g}}(p) - h_{\mathrm{sat,l}}(p)} \frac{1}{\Theta} = \frac{\dot{m}_\mathrm{l}}{\rho}. \tag{7}$$

While the original model parameters show a wide application range [20], they might require case specific adaptions, especially for only slightly superheated or cavitating flows [20, 21]. As the investigated cases have a low superheat, which can lead to a delayed vapor formation, the constant Θ_0 is set after a short study to $\Theta_0 = 1 \times 10^{-6}$ s.

Results and discussion

Analysis of the Experimental Visualisation

The high-speed shadowgraph images of the lowly superheated LN2 sprays #1, #6, #9 and #14 are depicted in Figure 4. As summarized in Table 1, the sprays #1 and #9 only differ in their injection pressures p_{inj} while the other injection parameters T_{inj} and p_{ch} remained constant. Hence, the degree of superheat R_p according to its definition in Equation 1 stays constant as well. However, a comparison of the shadowgraph images of the two sprays obviously reveals two different spray patterns despite their identical degrees of superheat: While spray #1 has a slim shape with distinct filaments and droplets, the spray pattern of spray #9 is wider and the spray appears to be more finely atomized. This can be quantified by comparing the spray angles θ_s of the sprays with each other which were extracted from the shadowgraph images in our former publication [15]: While spray #1 has a spray angle of $\theta_\mathrm{s} = 106.0\,°$ after a distance of $L/D = 1$ from the injector, the one of spray #9 is $\theta_\mathrm{s} = 117.5\,°$ which is about 11 % higher.

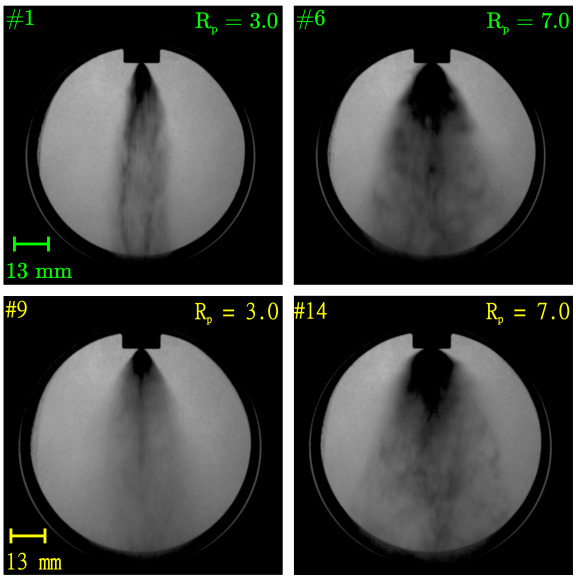

Figure 4. Shadowgraph images of stationary LN2 sprays #1, #6, #9 and #14 at $t_{inj} = 120$ ms after valve opening

The halving of the injection pressure from $p_{inj} \approx 800$ kPa in spray #1 to $p_{inj} \approx 400$ kPa in spray #9 leads to a reduction of the mass flow. Hence, the residence time of the fluid in the injector is increased for the spray #9 which enhances nucleation already within the injector and explains

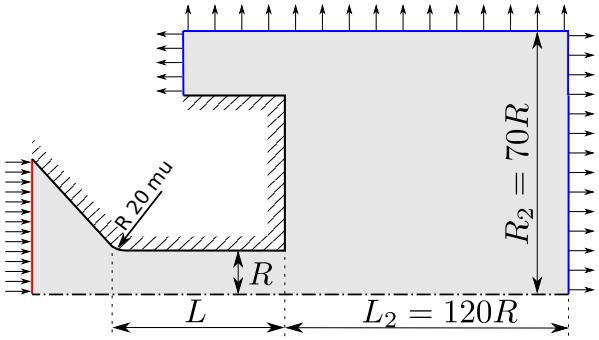

Figure 5. Sketch of the computational domain for the 2D wedge simulations.

Table 3. Residual times of the fluid inside the injector.

Case	Residual Time in Injector
#1	0.073 ms
#6	0.073 ms
#9	0.120 ms
#14	0.118 ms

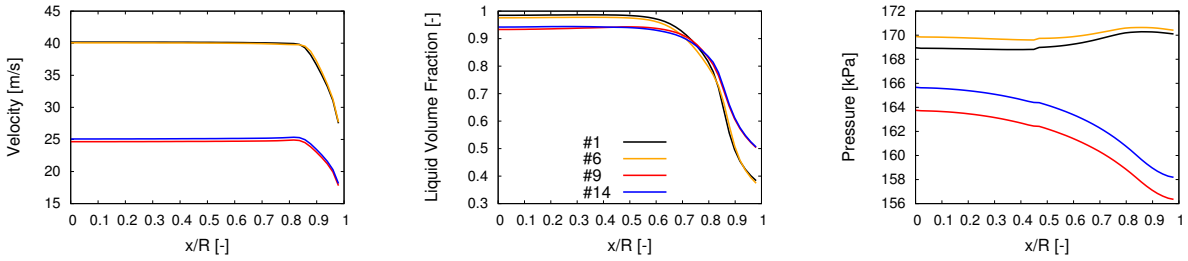

(a) Velocity (b) Liquid volume fraction (c) Pressure

Figure 6. Velocity, liquid volume fraction and pressure sampled at the exit of the nozzle.

the wider and better atomized spray compared to spray #1.

For higher degrees of superheat like $R_p = 7.0$ in the sprays #6 and #14, the same effects are still present but less pronounced. This is due to the higher amount of superheat which generates already high nucleation rates for both sprays. For those two sprays, the spray angle of spray #14 with $\theta_s = 153.7°$ is about 7 % higher than the one of spray #6 with $\theta_s = 144.1°$.

Numerical Analysis of the Spray Kinematics

An analysis of the nozzle exit velocity, liquid volume fraction and pressure is depicted in Figure 6. The velocity development is for the cases #9 and #14 about 40% less than for the cases with the higher injection pressure, which is in agreement with the experimental mass flow rates. Figure 6b shows, that the liquid volume fraction is reduced for the cases #9 and #14 which is due to the longer residual time in the injector, see Table 3. The lower volume fraction of cases #1 and #6 at the wall is a consequence of the increased flow separation at the inlet of the nozzle. This causes a more pronounced vena contracta and with it a larger low pressure region for cavitation. Finally, the pressure is for all cases slightly below the saturation pressure and thus not affected by the injection pressure or the downstream conditions. For the lower injection pressure cases the exit pressure is slightly lower because of the enhanced evaporation and with it cooling of the liquid. In conclusion this supports the claim, that the upstream conditions of injection pressure and liquid temperature determine the velocity and evaporation within the injector. Hence, the value R_p which does not include the injection pressure, cannot fully describe the behavior within the injector and with it the initial kinetic as well as thermodynamic state.

Conclusions

The degree of superheat in flash boiling sprays has a significant influence on the spray morphology, especially in terms of the spray widening and its atomization. However, the commonly used definition of the degree of superheat R_p has proved to be insufficient to predict the spray

patterns of lowly superheated LN2 sprays since it does not include the injection pressure and therefore neglects the initial kinetic states of the liquid within the injector. Hence, modified or different definitions of the degree of superheat have to be found or developed for a sufficient description of the flash boiling process.

Acknowledgements
We kindly acknowledge the financial support by the Deutsche Forschungsgemeinschaft (DFG, German Research Foundation) within the project SFB-TRR 75, project number 84 292 822.

Nomenclature

α	liquid volume fraction [-]
β	exponent of HRM model [-]
ΔT^*	degree of superheat [-]
λ	exponent in HRM model [-]
ρ	mixture density [kg m^{-3}]
$\boldsymbol{\tau}_t$	turbulent viscous stress tensor [kg s^{-2} m^{-1}]
θ	relaxation time for HRM model [s]
θ_s	spray angle [°]
D_{inj}	injector diameter [10^{-3} m]
g	gravitational constant m s^{-2}
h	enthalpy [J kg^{-1}]
h_sat	saturation enthalpy [J kg^{-1}]
Ja	Jacob number [-]
K	kinetic energy [J kg^{-1}]
$k_{l,\mathrm{Eff}}$	effective thermal conductivity [kg m s^{-3} K^{-1}]
L/D	length-to-diameter ratio [-]
$\dot{m}$	mass flow [g/s]
Oh	Ohnesorge number [-]
p_a	ambient pressure [kPa]
p_{ch}	chamber pressure [kPa]
p_{inj}	injection pressure [kPa]
p_{sat}	saturation pressure [kPa]
R_p	degree of superheat [-]
Re	Reynolds number [-]
T_{inj}	injection temperature [K]
t_{inj}	time after start signal for injection [s]
T_{sat}	saturation temperature [K]
$\boldsymbol{u}$	velocity vector [m s^{-1}]
We_g	gaseous Weber number [-]
We_l	liquid Weber number [-]

References

[1] Manfletti, C., 2014, Laser Ignition of an Experimental 400N Cryogenic Reaction and Control Thruster: Pre-Ignition Conditions, *J. Propul. Power*, 30 (4), pp. 925-933.
[2] Zeng, Y. and Lee, C.-F.F., 2001, An Atomization Model for Flash Boiling Sprays, *Combust. Sci. and Tech.*, 169 (1), pp. 45-67.
[3] Senda, J., Hojyo, Y. and Fujimoto, H., 1994, Modeling on Atomization and Vaporization Process in Flash Boiling Spray, *JSAE Review*, 15 (4), pp. 291-296.
[4] Senda, J., Wada, Y., Kawano, D. and Fujimoto, H., 2008, Improvement of Combustion and Emissions in Diesel Engines by Means of Enhanced Mixture Formation Based on Flash Boiling of Mixed Fuel, *Int. J. Engine Res.*, 9 (1), pp. 15-27.
[5] Elias, E. and Chambré, P.L., 1993, Flashing Inception in Water During Rapid Decompression. *J. Heat Transfer*, 115 (1), pp. 231-238.
[6] Cleary, V., Bowen, P. and Witlox, H., 2007, Flashing Liquid Jets and Two-Phase Droplet Dispersion: I. Experiments for Derivation of Droplet Atomisation Correlations, *J. Hazard. Mater.*, 142 (3), pp. 786-796.
[7] Yildiz, D., Rambaud, P, Van Beeck, J. and Buchlin, J.-M., 2002, A Study on the Dynamics of a Flashing Jet, “Final Contract Research Report EAR0030”. VKI.
[8] Lamanna, G., Kamoun, H., Weigand, B. and Steelant, J., 2014, Towards a Unified Treatment of Fully Flashing Sprays, *Int. J. Multiph. Flow*, 58, pp. 168-184.
[9] De Rosa, M., Sender, J., Zimmermann, H. and Oschwald, M., Sep. 2.-4. 2006, Cryogenic Spray Ignition at High Altitude Conditions, 42nd AIAA/ASME/SAE/ASEE JPC.
[10] Lamanna, G., Kamoun, H., Weigand, B., Manfletti, C., Rees, A., Sender, J., Oschwald,

M. and Steelant, J., 2015, Flashing Behavior of Rocket Engine Propellant, *At. Sprays*, 25 (10), pp. 837-856.

[11] Luo, M. and Haidn, O.J., 2016, Characterization of Flashing Phenomena with Cryogenic Fluid Under Vacuum Conditions, *J. Propul. Power*, 3 (5), pp. 1253-1263.

[12] Rees, A., Salzmann, H., Sender, J. and Oschwald, M., July 1.-4. 2019, Investigation of Flashing LN2-Jets in Terms of Spray Morphology, Droplet Size and Velocity Distributions, 8th EUCASS Conference.

[13] Rees, A., Araneo, L., Salzmann, H., Kurudzija, E., Suslov, D., Lamanna, G., Sender, J. and Oschwald, M., Sept. 2.-4. 2019, Investigation of Velocity and Droplet Size Distributions of Flash Boiling LN2-Jets With Phase Doppler Anemometry, 29th ILASS Europe Conference.

[14] Rees, A., Araneo, L., Salzmann, H., Lamanna, G., Sender, J. and Oschwald, M., 2020, Droplet Velocity and Diameter Distributions in Flash Boiling Liquid Nitrogen Jets by Means of Phase Doppler Diagnostics, *Exp. Fluids*, 61, pp. 182.

[15] Rees, A., Salzmann, H., Sender, J. and Oschwald, M., 2020, About the Morphology of Flash Boiling Liquid Nitrogen Sprays, *At. Sprays*, 30 (10), pp. 713-740.

[16] Rees, A., Salzmann, H., Sender, J. and Oschwald, M., March 17.-19. 2021, The Evolution of the Liquid Cores in Flash Boiling LN2 Sprays, 7th Space Propulsion 2020+1.

[17] Gärtner, J.W., Kronenburg, A., Rees, A., Sender, J., Oschwald, M. and Lamanna, G., 2020, Numerical and Experimental Analysis of Flashing Cryogenic Nitrogen, Int. J. Multiph. Flow 2020, 130, 103360.

[18] Bell, I.H., Wronski, J., Quoilin, S. and Lemort, V., 2014, Pure and Pseudo-Pure Fluid Thermophysical Property Evaluation and the Open-Source Thermophysical Property Library Coolprop, *Ind. Eng. Chem. Res.*, 53 (6), pp. 2498–2508.

[19] Downar-Zapolski, P., Bilicki, Z., Bolle, L. and Franco, J., 1996, The Non-Equilibrium Relaxation Model for One-Dimensional Flashing Liquid Flow, *Int. J. Multiph. Flow*, 22, pp. 473 – 483.

[20] Saha, K., Som, S. and Battistone, M., 2017, Investigation of Homogeneous Relaxation Model Parameters and their Implications for Gasoline Injectors, *At. Sprays*, 27 (4), pp. 345-365.

[21] Guo, H., Nocivelli, L., Torelli, R. and Som, S., 2020, Towards Understanding the Development and Characteristics of Under-Expanded Flash Boiling Jets, *Int. J. Multiph. Flow*, 129, 103315.